ELECTROCHEMISTRY

High-capacity aqueous zinc batteries using sustainable quinone electrodes

Qing Zhao,[1,2]* Weiwei Huang,[3]* Zhiqiang Luo,[1] Luojia Liu,[1] Yong Lu,[1] Yixin Li,[1] Lin Li,[1] Jinyan Hu,[3] Hua Ma,[4] Jun Chen[1,2]†

Quinones, which are ubiquitous in nature, can act as sustainable and green electrode materials but face dissolution in organic electrolytes, resulting in fast fading of capacity and short cycle life. We report that quinone electrodes, especially calix[4]quinone (C4Q) in rechargeable metal zinc batteries coupled with a cation-selective membrane using an aqueous electrolyte, exhibit a high capacity of 335 mA h g^{-1} with an energy efficiency of 93% at 20 mA g^{-1} and a long life of 1000 cycles with a capacity retention of 87% at 500 mA g^{-1}. The pouch zinc batteries with a respective depth of discharge of 89% (C4Q) and 49% (zinc anode) can deliver an energy density of 220 Wh kg^{-1} by mass of both a C4Q cathode and a theoretical Zn anode. We also develop an electrostatic potential computing method to demonstrate that carbonyl groups are active centers of electrochemistry. Moreover, the structural evolution and dissolution behavior of active materials during discharge and charge processes are investigated by operando spectral techniques such as IR, Raman, and ultraviolet-visible spectroscopies. Our results show that batteries using quinone cathodes and metal anodes in aqueous electrolyte are reliable approaches for mass energy storage.

INTRODUCTION

Developing high-performance rechargeable batteries is vital for regulating the energy output of intermittent solar and wind energy, which have been expected to occupy increasing proportions in energy distribution in light of the environmental issues caused by fossil energy (*1*–*3*). Batteries using organic electrodes are attractive electrochemical energy storage devices because organic compounds can be lightweight, environmentally friendly, and sustainable (*4*, *5*). In particular, quinone compounds are ubiquitous in nature, and the electrochemical reactions based on quinone and hydroquinone are indeed significant in biological electron transport systems (*6*, *7*). More than 2400 kinds of quinones have been discovered from angiosperms, fungi, marine animals, and insects. Inspired by nature, many artificial quinone compounds have also been designed for applications in medicine, molecular recognition, and organism electron/ion transfer (*8*). Currently, batteries using electroactive quinone electrodes mostly work with organic electrolytes, demonstrating fast fading of capacity due to the dissolution of active materials (*4*). Strategies such as electrolyte modification (*9*), polymerization (*10*), salt formation (*11*), and loading on substrates (*12*) have been used to improve the electrochemical performance. Applying quinone electrodes in aqueous batteries should be a smart choice to achieve stable electrochemical performance because quinones are barely soluble in water (*13*, *14*). Moreover, batteries operated with aqueous electrolytes are preferable in terms of safety (*15*–*17*).

Among the reported aqueous batteries, rechargeable zinc batteries (ZBs) are one of the most promising candidates because zinc anodes are affordable and exhibit high capacity (820 mA h g^{-1}), large production, and good compatibility with water (*18*–*21*). Up to now, great progress has been made on building high-performance ZBs using inorganic compounds such as metal oxides (*18*, *19*, *22*–*28*) and Prussian salts (*29*–*31*), in which Zn-MnO_2 battery systems are most widely studied. On the one hand, efforts on the MnO_2 cathode side largely focus on preparing high-capacity cathodes (*18*, *19*, *22*, *27*, *28*) and inhibiting dissolution of Mn^{3+} ions (*19*, *24*, *32*, *33*). Oh and Kim (*32*) discovered that the addition of various manganese (II) salts can increase the cycle stability of a MnO_2 cathode. Pan *et al.* (*19*) further reported that α-MnO_2 nanofiber cathodes could display long-cycle stability over 5000 cycles at a high rate of 5 C after inhibiting Mn^{3+} dissolution with $MnSO_4$ added to $ZnSO_4$ electrolyte. Yadav and co-workers (*27*, *28*) found that a Cu^{2+}-intercalated Bi–δ-MnO_2 cathode exhibited a capacity of 617 mA h g^{-1} (the theoretical second electron capacity) for over 6000 cycles against a Ni counter at 40 C and the same capacity for over 900 cycles against a Zn anode. On the other hand, strategies toward solving the problems of Zn anodes have also been tried (*34*, *35*). At high Zn utilizations, the shape change passivation and dendrite issues also plague the life of ZBs, which seems to be a large part of the problem of short-lived cells (*28*, *35*–*37*). Ito *et al.* (*38*) found that mesh-type anode current collectors with reduced areas were of potential interest for zinc deposition. Wei *et al.* (*39*) found that Bi and Cu substrates were suitable current collectors in zinc-anode alkaline rechargeable batteries. In addition, Zn is known to generate soluble ZnO_2^{2-} in alkaline Zn-MnO_2 batteries, which will poison the cathode and cause structure distortion (*28*, *40*, *41*). Bai *et al.* (*41*) demonstrated that an ion-selective separator can efficiently avoid cathode poisoning by preventing the diffusion of ZnO_2^{2-}. Calcium hydroxide layers have also been tried to trap zincate ions and address Zn blocking to avoid the structure distortion of MnO_2 (*28*, *40*).

As mentioned above, a considerable breakthrough has been made on rechargeable ZBs, especially with inorganic cathodes. However, to the best of our knowledge, organic quinone compounds are unexplored in ZBs. Quinone compounds have been tested as electrodes in aqueous electrolyte since 1972, in which tetrachlorobenzoquinone showed a reduction potential of 0.7 V in dilute H_2SO_4 solution (*42*). Meanwhile, quinone compounds have also been used as redox active materials in aqueous flow batteries (*43*). More recently, Liang *et al.* (*13*) reported universal quinone electrodes for aqueous (H^+, Li^+, Na^+, K^+, and Mg^{2+}) rechargeable batteries. These results show the versatile properties of quinone compounds in aqueous batteries, which make them potential candidates coupled with zinc anodes. In addition, quinone compounds can be lightweight, and the cations only act to

[1]State Key Laboratory of Elemento-Organic Chemistry and Key Laboratory of Advanced Energy Materials Chemistry, College of Chemistry, Nankai University, Tianjin 300071, China. [2]Collaborative Innovation Center of Chemical Science and Engineering, Nankai University, Tianjin 300071, China. [3]College of Environmental and Chemical Engineering, Yanshan University, Qinhuangdao 066000, China. [4]Tianjin EV Energies Company Limited (JEVE), Tianjin 300380, China.
*These authors contributed equally to this work.
†Corresponding author. Email: chenabc@nankai.edu.cn

compensate the charge of quinone-based electrochemical reactions, which can act as high-capacity cathodes in ZBs (*4*). The electrochemical process and structure evolution of inorganic electrodes are sufficiently studied through theoretical simulation and ex situ/in situ approaches such as x-ray diffraction (XRD) and transmission electron microscopy (TEM) (*44*). However, organic electrode materials with less crystallinity and stability are difficult to accurately characterize with these methods (*45*). Up to now, the fundamental studies on the reaction and dissolution of organic electrodes are limited and mainly based on ex situ methods. Exploring new theoretical methods combined with in situ experimental technologies that can deduce and operando-monitor the electrochemical reactions of organic electrodes are significant to better design the materials (*46*).

Inspired by the above points, we report a series of quinone compounds as high-performance cathodes in aqueous ZBs. Among them, the calix[4]quinone (C4Q) with open bowl structures and eight carbonyls exhibits a high capacity of 335 mA h g^{-1}, a flat and safe operation voltage of 1.0 V, and a low polarization of 70 mV with high energy efficiency of 93% at low current density. A long life of 1000 cycles with 87% capacity retention is achieved at a current density of 500 mA g^{-1}. Meanwhile, the electrostatic potential (ESP) method was applied to calculate the active centers of quinone electrode materials, illustrating that the carbonyl groups are the reactive sites. In situ technologies of attenuated total reflection–Fourier transform IR (ATR-FTIR) spectroscopy, Raman spectroscopy, and ultraviolet-visible (UV-vis) spectroscopy were also developed to monitor the electrochemical reaction on quinone electrodes in real time. A cation-exchange membrane (Nafion) was introduced as a separator into aqueous ZBs to suppress the dissolution of the active materials and protect the zinc anode from poisoning by discharged products. These safe and high-capacity aqueous ZBs are promising electrochemical devices for reliable energy storage and conversion.

RESULTS

The quinone electrodes in aqueous ZBs

We selected various quinone compounds with carbonyls in para-position [1,4-naphthoquinone (1,4-NQ), 9,10-anthraquinone (9,10-AQ) and C4Q] and ortho-position [1,2-naphthoquinone (1,2-NQ) and 9,10-phenanthrenequinone (9,10-PQ)] as cathodes in aqueous ZBs (fig. S1). Among them, C4Q was synthesized with raw materials of calix[4]arene and *p*-aminobenzoic acid (Fig. 1A) (*9*). Calix[4]arene with unique cavity structures is extensively used as a precursor in areas of molecular recognition, sensor, ion carrier, mimic enzyme, and phase transfer catalysis (*47*). *P*-aminobenzoic acid as a major component of folic acid is widely distributed in yeast and bran. The complete procedure of preparation is facile under low temperature (<100°C), and the products are degradable. Meanwhile, the purification of products only includes a recrystallization process without requiring a chromatographic procedure, making production easily scalable.

All selected quinone electrodes are feasible for highly reversible Zn ion uptake (fig. S2). It should be mentioned that we describe Zn ions briefly because the pH of the electrolyte is about 3.6 (*24*), in which the dissolved zinc is actually present as Zn^{2+} surrounded by six H_2O molecules {$[Zn(H_2O)_6]^{2+}$} (*48*). The results indicate that the quinone compounds with carbonyls (C=O double bond) in para-position (1,4-NQ, 9,10-AQ, and C4Q) generally show higher capacity and lower charge/discharge gap than those with carbonyls in ortho-position (1,2-NQ and 9,10-PQ) (Fig. 1B). The ortho carbonyls in quinones would cause larger steric hindrance for Zn ion reactions, thus showing worse electrochemical performance. Furthermore, the working potential of different quinones is highly related to the energy of the lowest unoccupied molecule orbital (LUMO). Lower LUMO energy indicates higher discharge potential (*49*). The order of average discharge potential is 9,10-AQ < 9,10-PQ < 1,4-NQ < 1,2-NQ < C4Q, which agrees with theoretical calculations (fig. S3). In particular, the cathode of C4Q displays a capacity of 335 mA h g^{-1}, corresponding to uptake of three Zn ions and utilization of six carbonyls (Fig. 1C). This value is far exceeds most reported electrodes in aqueous Li/Na ion batteries (*15*) and can also act as one of the best in aqueous ZBs (Fig. 1B and table S1) (*18*–*20*, *22*–*31*). In addition, the voltage gap between discharge and charge is only 70 mV, contributing to the high energy efficiency of ~93% for the first five cycles (Fig. 1C). The flat discharge platform contributes to the stable energy output, which can simplify the procedure of voltage regulation in practical application. In aqueous-based batteries, the galvanostatic curves are usually decided by phase reaction mechanisms. Therefore, the flat plateau characteristics of Zn-C4Q batteries are supposed to be the heterogeneous two-phase reactions (*50*). It is worth noting that the 9,10-AQ electrode displays a capacity of 194 mA h g^{-1} with even a narrower charge/discharge gap of 40 mV. The flat and low discharge platform at 0.51 V makes it appealing as an anode in aqueous batteries.

Cyclic voltammetry (CV) curves at different scan rates have been carried out to clarify the controlling factors of the electrochemical reactions (*51*). One reduction peak corresponds to the reaction from C4Q to Zn_3C4Q, and one oxidation peak corresponds to the reaction from Zn_3C4Q to C4Q, respectively (Fig. 1D). When the scan rate increases, the reduction peak shifts to lower potential, and the oxidation peak shifts to higher potential owing to the increased polarization. The peak current enhances linearly with the square root of the scan rate (inset of Fig. 1D), indicating that the Zn ion uptake and removal behavior are controlled by the diffusion process. Moreover, the electrochemistry of Zn and C4Q is highly reversible without any obvious change after 100 cycles of CV (fig. S4). This diffusion process is also demonstrated by other quinone electrodes of 9,10-PQ and 9,10-AQ (fig. S5).

Theoretical calculations and operando characterizations of quinone electrodes in ZBs

Theoretical calculations with density functional theory (DFT) were conducted to deduce the structure evolution of C4Q before and after Zn ion uptake (*52*). Because of C–C single bond that connects each benzoquinone unit, the C4Q exhibits a bowl-like structure endowed with small steric hindrance. The two carbonyls on the top and four carbonyls on the bottom are adjacent. To analyze the exact sites of Zn ion uptake, the ESP approach, which is often applied to deduce the electrophilic or nucleophilic reaction in organic chemistry, has been used to deduce the active sites of organic electrodes (*53*). The sites with more positive ESP tend to occur in nucleophilic reactions, whereas the more negative ESP areas prefer electrophilic reactions (*53*). Because the discharge process of the batteries involves Zn ion uptake, the sites with more negative ESP are attractive for discharge reactions. According to the results of ESP mapping, the regions near the carbonyls of quinones have more negative ESP values, which are considered highly reactive sites (Fig. 2, A to D). For the C4Q molecular structure, the carbonyls on and under a molecule of C4Q are more favorable for Zn ion uptake because they display lower ESP than the bilateral carbonyls (Fig. 2E). The number of Zn ion uptakes for each C4Q is three (Fig. 2F). According to the change of calculated Gibbs free energy, the reaction of C4Q + 3Zn = Zn_3C4Q occurs at 0.91 V, which is close to the practical

discharge potential (1.0 V). At the top of C4Q where there are two carbonyls, the distance between Zn and each of two O atoms is both 1.83 Å. At the bottom of C4Q, where there are four carbonyls, the distance between Zn and two of the nearer carbonyl O atoms is 1.88 Å, and the distance between Zn and the other two relatively distant O atoms is 2.50 Å. These distances demonstrate that the Zn ions have strong interaction with two carbonyls at the top and four carbonyls at the bottom (*54*). When the fourth Zn ion uptake was considered, two possible geometrical configurations of Zn_4C4Q were calculated. One is when Zn ion uptake occurs at the top of Zn_3C4Q (fig. S6A), and the other is when Zn ion uptake occurs on the side chain of Zn_3C4Q (fig. S6B). These two configurations correspond to theoretical discharge plateaus of 0.08 and 0.03 V, respectively, indicating difficulties for the formation of Zn_4C4Q. The DFT calculations results are also in accordance with the capacity of the experiment. Note that in the more stable configurations of the above two structures (as is shown in fig. S6A), the fourth Zn has moved away from the C4Q because of the geometrical optimization process. After full optimization, the distance between the fourth Zn and the nearest O is as far as 3.56 Å, indicating no Zn–O bond formation. Moreover, even at an extremely low current density, the capacity is still about 337 mA h g^{-1} (discharge time continues for over 60 hours), corresponding to the third Zn ion uptake (fig. S7). Prominently, both the configuration and volume of C4Q show little change after the third Zn ion uptake, contributing to the low polarization of Zn-C4Q batteries.

To further confirm the active center of C4Q, we designed an ATR-FTIR battery to investigate the variation of quinone with Zn ion uptake/removal. A tailored stainless steel mesh is used to load the C4Q cathode in which

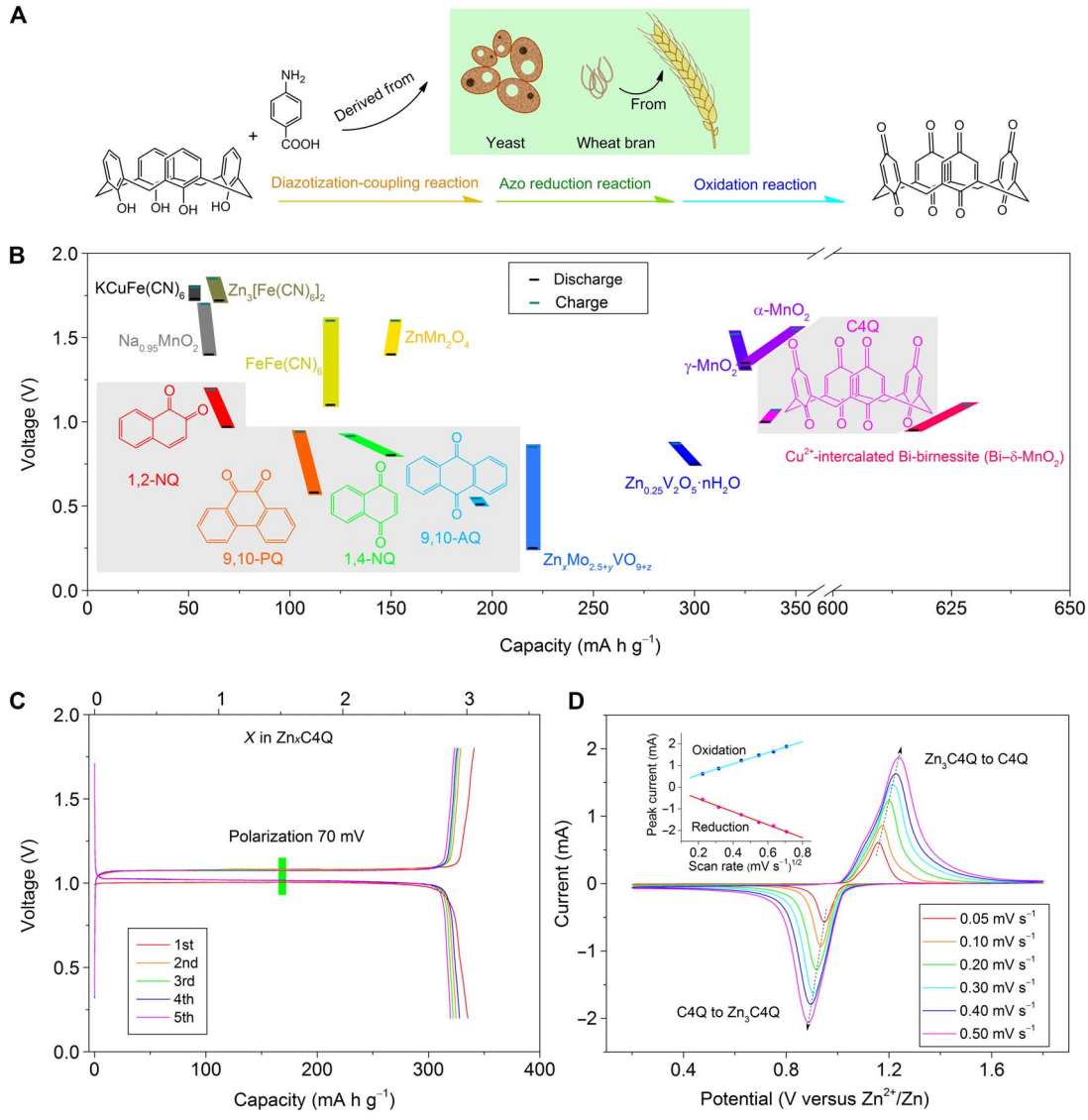

Fig. 1. Quinone electrodes in aqueous ZBs. (**A**) Schematic diagram of preparing C4Q. (**B**) Discharge/charge voltages and capacities of selected quinone compounds (1,2-NQ, 1,4-NQ, 9,10-PQ, 9,10-AQ, and C4Q) in aqueous ZBs. The typically reported inorganic electrodes including $KCuFe(CN)_6$ (*31*), $Na_{0.95}MnO_2$ (*26*), $Zn_3[Fe(CN)_6]_2$ (*30*), $FeFe(CN)_6$ (*29*), $ZnMn_2O_4$ (*24*), $Zn_xMo_{2.5+y}VO_{9+z}$ (*25*), $Zn_{0.25}V_2O_5{\cdot}nH_2O$ (*23*), γ-MnO_2 (*22*), α-MnO_2 (*19*), and Cu^{2+}-intercalated Bi-birnessite (Bi–δ-MnO_2) (*27*, *28*) are also listed for comparison. (**C**) Galvanostatic discharge/charge curves of Zn-C4Q battery at the current density of 20 mA g^{-1}. The upper *x* axis represents the uptake number of Zn ions. One Zn^{2+} with two-electron transfers generates a specific capacity of 112 mA h g^{-1}. (**D**) CV curves of Zn-C4Q batteries at sweeping rates of 0.05, 0.10, 0.20, 0.30, 0.40, and 0.50 mV s^{-1}, respectively. The reduction and oxidation peaks are linked with arrows. The inset shows the corresponding linear fit of the peak current and the square root of the scan rate.

the infrared (IR) light is able to push through the cathode and obtain the IR spectroscopy (Fig. 3A). The stretching vibration of carbonyl is at about 1650 cm^{-1}. With the in-depth process of discharging, the intensity of the carbonyl vibration peak declines, indicating the reaction between Zn ions and carbonyl. The intensity rises again to a high level after the charging process, indicating the removal of the Zn ion from C4Q (Fig. 3, B and C). In comparison, another characteristic peak located at about 1300 cm^{-1} belongs to the stretching vibration of CH_2, a connecting benzoquinone unit (*9*), which is nearly unchanged in discharge and charge processes. Meanwhile, in situ Raman spectra present the same structural evolution (fig. S8A). The peaks at a Raman shift of about 1670 cm^{-1} can be assigned to the C=O bond, becoming very weak after full discharge and reverting to the original intensity after full charge (*55*). These results illustrate that the redox center of C4Q is carbonyl. In addition, ex situ XRD patterns demonstrate the high reversibility of crystal structures after Zn ion removal (fig. S9) (*56*). After fully discharging, zinc is homogeneously distributed in the C4Q cathode (fig. S10). It is worth noting that O and C are homogeneously distributed in the fully charged C4Q cathode without any zinc, indicating the removal of Zn after the charge process (fig. S11). After a long-term cycling, the cathode materials still show good reversibility according to the results of FTIR spectroscopy, (Fig. 3B), Raman spectroscopy (fig. S8B), and XRD (fig. S9).

Electrochemical performance optimization

Two different separators, filter paper and a cation-selective membrane (Nafion; fig. S12), have been used to test the electrochemical properties of C4Q in aqueous ZBs. The typical loading of active materials is ~2.5 mg cm^{-2}, leading to the areal capacity of ~0.8 mAh cm^{-2} and zinc utilization of ~4% (fig. S13). The capacity still remains about 90% at the loading mass up to 10 mg cm^{-2}, at which point the zinc utilization increases to 15% (fig. S14). The Nafion membrane was initially soaked in the electrolyte over 1 day before use. After soaking, the zinc is uniformly distributed in the cross section of the Nafion membrane (Fig. 4A). The soaked membrane was directly used as both separator and electrolyte. The symmetric Zn/Nafion/Zn batteries demonstrate that the Nafion membrane is stable and fast for Zn ion diffusion. The gap between Zn plating and Zn stripping is still only 70 mV after cycling for 800 hours (Fig. 4B). The dissolution in organic electrolyte of electroactive quinone electrodes has been known as a serious drawback, hindering their practical application. As a result, the C4Q cathode applied in ZBs with organic electrolyte undergoes rapid decay (fig. S15). The raw quinone compounds are scarcely soluble in water, making the quinone electrodes in aqueous batteries display much better cycling performance. However, the slight solubility of quinone salts (discharge product) accompanied by its possible side reaction on zinc anode has to be considered for long-life cycling. The uptake of Zn ions will ionize the C4Q with formation of Zn_xC4Q. Then, the dissociation of Zn_xC4Q to Zn^{2+} and $C4Q^{2x-}$ makes it more soluble than C4Q. The dissolved $C4Q^{2x-}$ in the electrolyte can pass through the filter paper and react with zinc, forming a by-product on the anode side (fig. S16). Both the by-product formation and the dissolution of the discharge product cause the decline of capacity. The by-product on the anode side belongs to the species of Zn_xC4Q according to the results of FTIR spectroscopy and XRD (fig. S17). In comparison, the Nafion membrane is ion-selective and only permits

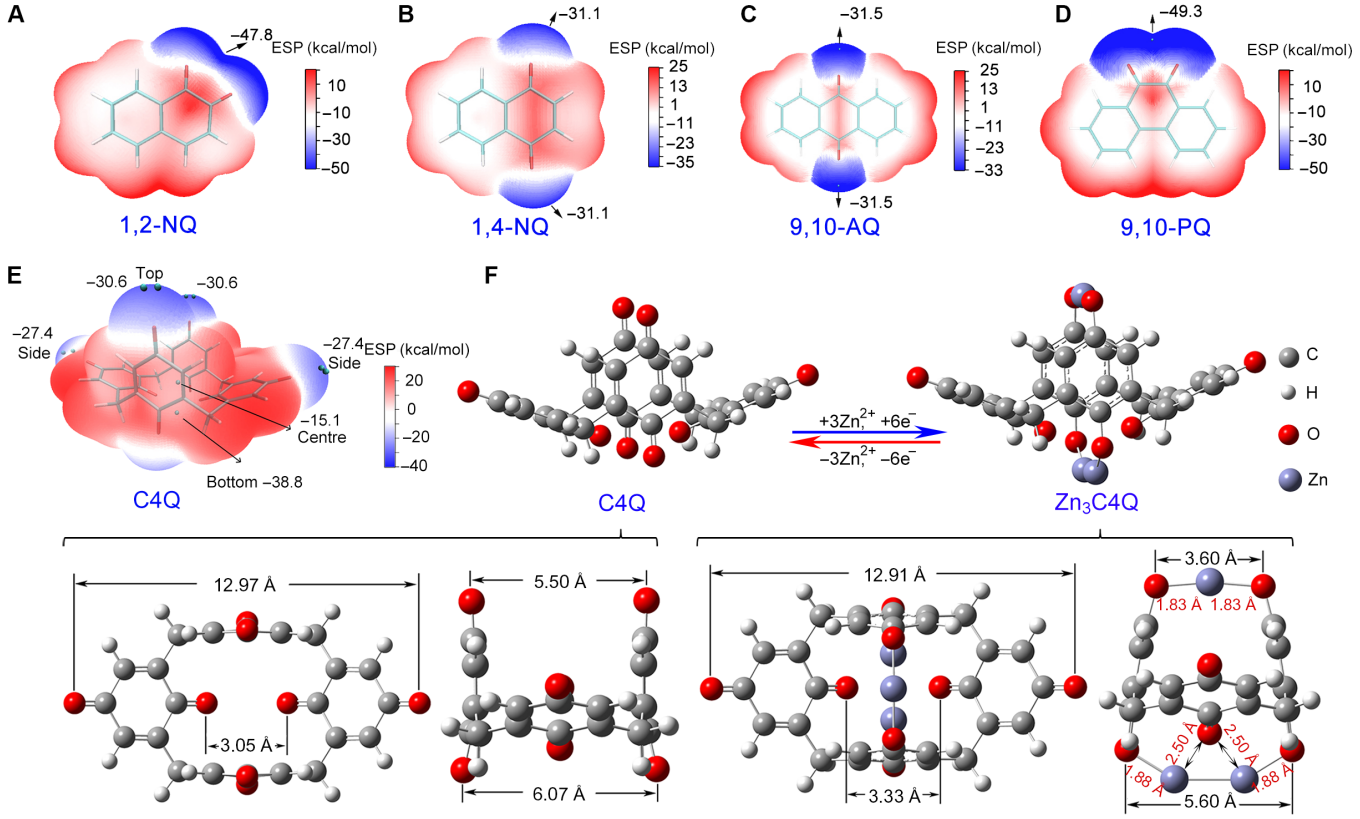

Fig. 2. Deducing the active sites and structure evolution of quinone electrodes. The ESP- mapped molecular van der Waals surface of (**A**) 1,2-NQ, (**B**) 1,4-NQ, (**C**) 9,10-AQ, (**D**) 9,10-PQ, and (**E**) C4Q. Surface local minima of ESP are represented as blue spheres, and the corresponding ESP values are marked out by numbers. (**F**) Optimized configurations of C4Q before and after Zn ion uptake. Bottom: Corresponding configurations at different viewpoints. The distance between O–O and Zn–O has been labeled in angstroms.

the cation to cross (*57*). Therefore, the batteries with the Nafion membrane show much more stable cycling performance owing to the prevention of anions from crossing. The capacity retention is 93% after 100 cycles (Fig. 4C). Furthermore, the morphology evolution shows the protection of the Zn anode without the generation of the by-product (fig. S18). Moreover, after 1000 cycles at 500 mA g^{-1}, the capacity retention is still 87%, which only declines at 0.015% per cycle (Fig. 4D). The Zn-C4Q batteries with the Nafion separator also display decent rate performance. The specific capacities at the current densities of 50, 100, 250, 500, 750, and 1000 mA g^{-1} are 333, 273, 220, 197, 174, and 172 mA h g^{-1}, respectively (fig. S19). The high current density will increase the polarization to ~200 mV, resulting in a reduced energy efficiency of about 80% (fig. S20). The reason for fading of capacity at high current density is the low conductivity of quinone materials. After increasing the weight ratio of Super P conductive additive, the capacity remains 215 mA h g^{-1} after 100 cycles at 500 mA g^{-1} (fig. S21).

To demonstrate the prospect of large-scale application, we assembled pouch cells for galvanostatic tests. As illustrated in Fig. 4E, the pouch ZBs are fabricated with multilayered stacking configurations (digital photos; fig. S22) (*58*). The energy density of the pouch cell is ~220 Wh kg^{-1} by the mass of electrodes (C4Q and theoretically used zinc metal, calculation in the Supplementary Materials) and ~80 Wh kg^{-1} by the total mass of the pouch, far exceeding that of commercial aqueous lead-acid batteries (~40 Wh kg^{-1}). Moreover, the pouch cells are packaged under atmospheric environment and operate at a narrow voltage window, which facilitates large-scale integration. The voltage plateaus are basically maintained at ~1.0 V for the pouch cells. However, fading of capacity begins to occur within 10 cycles due to high zinc utilization (close to 50%) of the designed pouch batteries (fig. S23). Although optimization such as protection of zinc anodes at high utilization is still needed for long-time cycling, these preliminarily tests demonstrate that aqueous ZBs with quinone electrodes are promising for safe and reliable energy storage.

Dissolution behavior characterization

To give insight into the distinction of electrochemical performance between filter paper and a Nafion membrane, we developed an in situ UV-vis spectroscopy technology to observe the dissolution of redox species in aqueous electrolyte (fig. S24). For batteries with the Nafion membrane that is closely attached to the C4Q cathode, only weak absorption peaks emerge and the electrolyte remains clear after cycling, proving the suppression of dissolution (Fig. 5A and fig. S25). The nearly unchanged

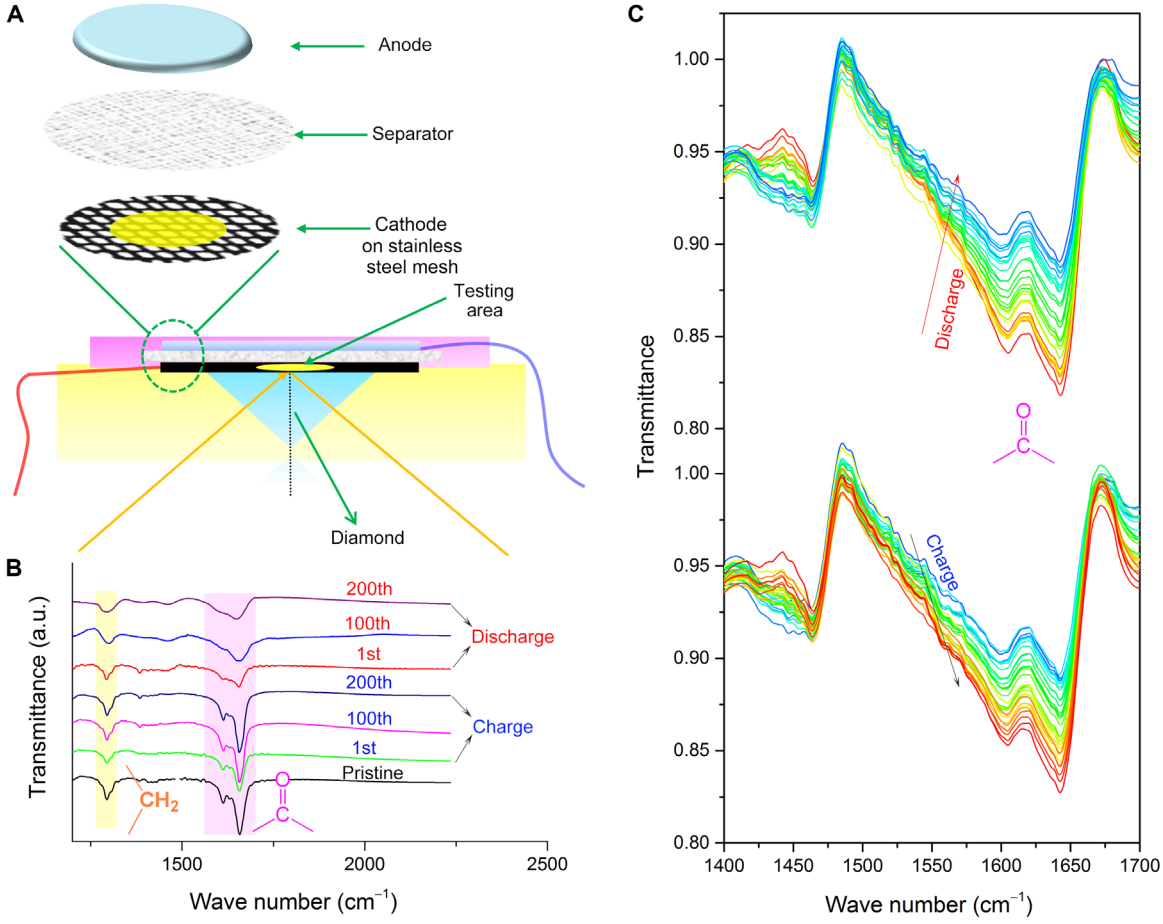

Fig. 3. FTIR characterization of quinone electrodes. (**A**) Schematic diagram of in situ ATR-FTIR analysis. The cathode was tightly pressed on the surface of the diamond. When the IR light reflects on the surface of the cathode, it will penetrate a certain depth of sample and obtain the FTIR spectra. (**B**) FTIR spectra of a pristine, 1st charged, 100th charged, 200th charged, 1st discharged, 100th discharged, and 200th discharged C4Q cathode. a.u., arbitrary units. (**C**) In situ ATR-FTIR spectra of the C4Q cathode in one discharge/charge cycle (the current density is 20 mA g^{-1}). The peaks at around 1650 cm^{-1} were assigned to the stretching vibration of carbonyls.

UV-vis curves also prove that the concentration and composition of the electrolyte are stable with cycling. In comparison, the electrolyte of the batteries without Nafion coating turns light yellow after cycling with the gradually enhanced UV-vis adsorption peaks, being ascribed to the dissolution of discharge products in the electrolyte (Fig. 5B). The peaks in the UV-vis test correspond to soluble species of $C4Q^{2x-}$ in discharge products, which is further proved by nuclear magnetic resonance (NMR) spectra using deuterium oxide (D_2O)–based electrolyte (fig. S26). To characterize the Zn^{2+} transmission ability of the Nafion membrane, we tested the membrane potential of C4Q. The membrane potential is 12 mV and the corresponding Zn ion transmission number is 0.83, indicating the excellent cation selectivity and fast Zn^{2+} transmission ability of adoptive Nafion membrane (fig. S27) (*59*, *60*). Electrochemical impedance spectroscopy (EIS) presents the resistance variation with different separators (fig. S28). The resistances of batteries with the Nafion membrane show little change with cycling, whereas both the solid electrolyte interface and charge transfer resistance with the filter paper separator increases apparently. This phenomenon is supposed to be caused by the dissolution of discharge products and by-product generation at the anode side.

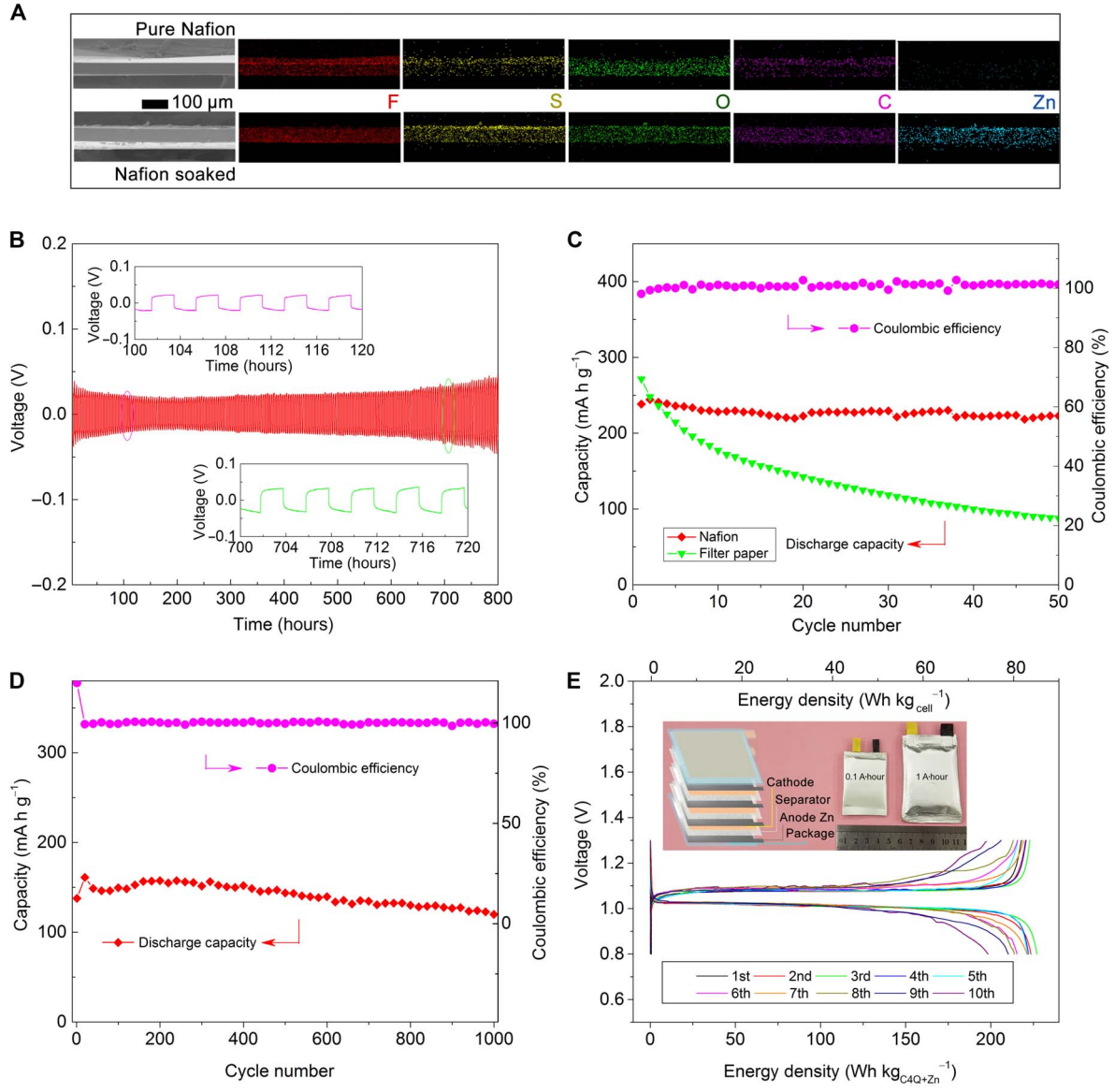

Fig. 4. Electrochemical performance optimization of aqueous Zn-C4Q batteries. (**A**) Scanning electron microscopy (SEM) images and corresponding energy dispersive x-ray spectroscopy mapping of the cross-sectional view of a Nafion membrane before (up) and after (low) electrolyte soaking. (**B**) Discharge/charge curves of a symmetric Zn/Nafion/Zn battery at a current density of 50 μA cm^{-2} and discharge/charge for 2 hours at each cycle. (**C**) Cycling performance of Zn-C4Q batteries with the Nafion membrane or filter paper as separators at the current density of 100 mA g^{-1}, accompanied with the coulombic efficiency with the Nafion membrane. (**D**) Cycling performance of Zn-C4Q batteries and coulombic efficiency at the current density of 500 mA g^{-1} with a Nafion separator. (**E**) Galvanostatic discharge/charge curves of pouch cells. Both energy densities calculated by electrodes (C4Q cathode and theoretical Zn anode) and by the total battery have been labeled on the bottom and top of the *x* axis. The inset shows the packaging technology and assembled pouch cell with a standard capacity of 0.1 and 1 A · hour, respectively.

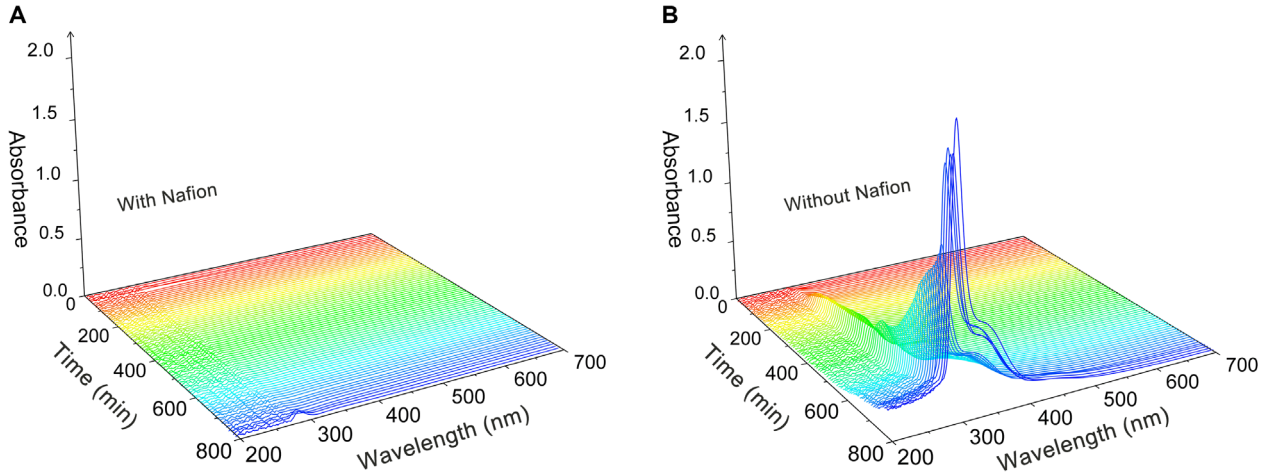

Fig. 5. Dissolution behavior of aqueous ZBs. (**A**) In situ UV-vis spectra of Zn-C4Q batteries with a Nafion separator. (**B**) In situ UV-vis spectra of Zn-C4Q batteries without a Nafion separator. These reformed batteries were discharged and charged at the current density of 100 mA g^{-1}, and the UV-vis spectra were collected every 10 min.

The above results demonstrate that quinone electrodes have shown great potential in aqueous ZBs. In addition to coupling with metal zinc, Mg, being a lightweight metal, can also be applied as an anode in aqueous batteries. In that case, the working voltage can be further elevated because of the lower standard potential of Mg^{2+}/Mg. A preliminary test of a Mg-C4Q battery shows a capacity of 247.4 mA h g^{-1} with a discharge potential of 1.54 V (fig. S29). Furthermore, the DFT calculations also demonstrate the stability of C4Q after the third Mg-ion uptake (fig. S30), and the fourth Mg ion uptake occurs at about 0.4 V. The calculated average discharge potential is about 1.8 V, which is close to the result of the experiment (fig. S30). Meanwhile, other calix quinone compounds, such as calix[6]quinone and calix[8]quinone, with similar structures are also potentially high capacity cathodes in aqueous batteries. More exciting progress can be anticipated on this field using quinones and other organic compounds.

DISCUSSION

Through using multicarbonyl quinone compounds composed of naturally abundant elements (C, H, and O), we have enriched the family of electrode materials for aqueous ZBs. The sustainable organic electrodes display a high capacity of 335 mA h g^{-1} and a low charge/discharge potential gap of 70 mV at 20 mA g^{-1}. The cycling stability is up to 1000 times with 87% capacity retention at 500 mA g^{-1}. The pouch cells deliver a flat operation voltage of 1.0 V with an energy density of 220 Wh kg^{-1} by the mass of C4Q and theoretically used zinc metal (corresponding to 80 Wh kg^{-1} by the total mass of pouch cells). Moreover, the combination of theoretical simulation and experimental in situ FTIR and Raman spectra demonstrates that carbonyls with more negative ESP are active centers for Zn ion storage. The operando UV-vis spectra show that ion-selective membranes can inhibit the dissolution of discharge products and protect zinc anodes from poisoning by quinones in aqueous ZBs. These technologies are also promising for the characterization of other materials. These organic material–based aqueous metal (Zn and Mg) batteries have produced interesting topics. Through elaborately designing the molecular structure, we predict that more organic materials with higher capacity and voltage will be available in further studies.

MATERIALS AND METHODS

Material preparation

The C4Q was prepared from the raw materials of calix[4]arene (*9*). The diazotization-coupling reaction took place on *p*-aminobenzoic acid to generate the compound of 5,11,17,23-tetrakis[(*p*-carboxyphenyl)azo]-25,26,27,28-tetrahydroxycalix[4]arene (compound 1). After azo reduction reaction, compound 1 was transferred into 5,11,17,23-tetrakis [(*p*-carboxyphenyl)azo]-25,26,27,28-tetrahydroxycalix[4]arene (compound 2). Finally, compound 2 was further oxidized and C4Q was obtained. The characterizations of C4Q (yellow powders) were as follows: IR spectra, 1650, 1613, 1296 cm^{-1}; ^{1}H NMR, 3.47 parts per million (ppm) (CH_2-, s, 2H) and 6.70 ppm (CH=C-, s, 2H); ^{13}C NMR, 30.4, 134.2, 146.6, 185.3, and 187.2 ppm; elemental analysis: C, 69.91 weight % (wt %); H, 3.49 wt %; electrospray ionization mass spectrometry (mass/charge ratio): [M], 480.4; found: $[M+Cl]^-$, 514.8; density, 1.6 g cm^{-3}; and SEM image, microrods. Other quinone compounds (1,2-NQ, 1,4-NQ, 9,10-PQ, and 9,10-AQ) are commercially available.

Battery testing

The electrodes were prepared with C4Q, Super P conductive additives, and polyvinylidene fluoride with a weight ratio of 6:3.5:0.5. 1-Methyl-2-pyrrolidinone was used as a dispersing agent. The mixed slurry was smeared on a thin titanium foil or stainless steel and dried in an oven at 80°C for 12 hours. The loading mass of C4Q ranged from 2.5 to 10 mg cm^{-2} for coin cells and about 10 mg cm^{-2} at each side of the Ti foil for pouch cells. The typically used Ti foil current collector was ~25 μm (round piece with a diameter of 10 mm), and the thickness of the active materials on the Ti foil was ~48 μm. The electrodes of commercial 1,2-NQ, 1,4-NQ, 9,10-AQ, and 9,10-PQ were fabricated under the same conditions. Zn foil was applied as a counter electrode. The typical weight of Zn foil is 13 mg cm^{-2}, and its thickness was ~20 μm (round piece of zinc with a diameter of 14 mm). The electrolyte was 3 M $Zn(CF_3SO_3)_2$ aqueous solution. A Nafion membrane was pretreated at 80°C step by step with 4 wt % H_2O_2 aqueous solution for 0.5 hour, distilled water for 0.5 hour, 0.8 M H_2SO_4 for 0.5 hour, and H_2O for 0.5 hour. The treated Nafion membrane was impregnated in electrolyte for 2 days and used as the separator without further electrolyte addition. In comparison, the commercial filter paper was also applied as a separator. The filter paper was

composed of fiber and the ash content was less than 0.1%. The pore of the filter paper was 30 to 50 μm provided by Wohua Filter Paper Limited Company (Hangzhou). Both coin 2032 and pouch cells were assembled for battery testing. The amount of electrolyte was about 50 μl for coin cell batteries in starved form using the filter paper separator. The galvanostatic discharge/charge tests were conducted on a LAND-CT2001A battery testing instrument. Cyclic voltammograms were obtained on Parstat 2263 electrochemical workstation (Princeton Applied Research and AMETEK Company). EIS was obtained on the Parstat 4000 electrochemical workstation with the frequency from 100 kHz to 10 mHz.

Characterization

Bruker TENSOR II was used to carry out the in situ ATR-FTIR test. To collect the IR spectra, we assembled a reformed battery in which a stainless steel mesh was applied as the current collector. The C4Q mixed with a small portion of Super P was then pressed on this current collector to fabricate the cathode. The cathode was first put on the diamond of TENSOR II, followed by a filter paper separator along with a small quantity of electrolyte. The zinc foil was then added to construct the final battery. This battery was fastened to the instrument for battery test and spectra collection. In situ Raman spectra were taken with a Thermo Fisher Scientific DXR Raman microscope with excitation at 638 nm from an argon ion. To let the laser light enter the battery, a small hole was drilled in the cathode shell, which was then covered with an Al_2O_3 optical glass. In situ UV-vis spectroscopy was performed on a JASCO V-550 UV/Vis spectrophotometer. The cuvette was reformed as an electrochemical tank. The reference cuvette was filled with the pure electrolyte. The Zn anode and cathode with or without a Nafion membrane were put into the working cuvette with the same electrolyte of 3 M $Zn(CF_3SO_3)_2$ aqueous solution for battery testing. XRD patterns were tested on Rigaku MiniFlex600 (Cu K_α radiation). The morphology was represented with the field-emission SEM (JEOL JSM7500F) and TEM (Philips Tecnai FEI).

The transmission number of Zn^{2+}

The transmission number of Zn^{2+} can be used to evaluate the capacity of ionic selectivity. A large value of the transmission number (close to 1) implies good ion selectivity, which can be calculated by the following equation

$$E^m = (2t_i^m - 1)\frac{RT}{nF}\ln\frac{\alpha_1}{\alpha_2} \quad (1)$$

where E^m is the tested membrane potential, t_i^m is the transport number of Zn^{2+}, and α_1 and α_2 are the mean activity of solution. The value of E^m can be tested from the instrument drawn in fig. S27 (12 mV). α_1 and α_2 are calculated as follows (*60*)

$$\alpha_1 = \gamma_1 C_1, \alpha_2 = \gamma_2 C_2 \quad (2)$$

$$\ln\gamma_\pm = -1.172|Z^+Z^-|\sqrt{I} \quad (3)$$

$$I = \frac{1}{2}\Sigma C_i Z_i^2 \quad (4)$$

where C is the concentration of ions and Z is the corresponding charge number. In this experiment, the solution on the left and right of the Nafion membrane are 1 mM and 5 mM $Zn(CF_3SO_3)_2$, respectively. The certain equation results are as follows:

1) Eq. 4: $I_{1mM} = 0.003$, $I_{5mM} = 0.015$.
2) Eq. 3: $\gamma_{\pm 1mM} = 0.8795$; $\gamma_{\pm 5mM} = 0.7504$.
3) Eq. 2: $\alpha_1 = 0.8795 \times 10^{-3}$; $\alpha_2 = 3.752 \times 10^{-3}$.
4) Eq. 1: $t_i^m = 0.83$.

The Zn^{2+} transmission number was 0.83 and close to 1, indicating high Zn^{2+} selectivity and transmission capacity.

Calculation details

DFT calculations were carried out with the Gaussian 09W software package to gain structural information of the abovementioned molecules. Geometrical optimization adopted the B3LYP method with 6-31+G(d,p) basis sets. On the basis of the optimized structure of a C4Q molecule, ESP analysis on van der Waals surface was done to deduce the possible Zn ion uptake positions using the Multiwfn 3.3.8 software package and the cubeman utilization in the Gaussian 09W software package. Gibbs free energies in water solution were calculated using an steered molecular dynamics solvent model, with the method and basis sets in consistence with geometrical optimization.

SUPPLEMENTARY MATERIALS

Supplementary material for this article is available at http://advances.sciencemag.org/cgi/content/full/4/3/eaao1761/DC1

fig. S1. Illustration of rechargeable aqueous ZBs using quinone electrodes.
fig. S2. Electrochemical properties of other quinone compounds.
fig. S3. LUMO energy and average discharge potential of different quinone compounds.
fig. S4. CV curves of Zn-C4Q battery at 0.5 mV s^{-1} for 100 cycles.
fig. S5. CV curves of other quinone compounds.
fig. S6. The uptake of the fourth Zn ion in the molecular structure of C4Q.
fig. S7. Discharge and charge curves of Zn-C4Q battery at 5 mA g^{-1}.
fig. S8. Raman characterizations of Zn-C4Q batteries.
fig. S9. Ex situ XRD characterizations of Zn-C4Q batteries.
fig. S10. TEM characterization of C4Q electrode after discharge.
fig. S11. TEM characterization of C4Q electrode after charge.
fig. S12. Composition of Nafion.
fig. S13. SEM images of the prepared C4Q cathode on titanium foil.
fig. S14. Capacity retention and zinc utilization using different loading masses of C4Q.
fig. S15. Electrochemical performance of Zn-C4Q batteries in organic electrolyte.
fig. S16. Digital photos of the Zn anode, separator (filter paper or Nafion membrane), and C4Q cathode after cycling.
fig. S17. Characterization of the zinc anode after cycling using a filter paper separator.
fig. S18. SEM images of electrodes before and after cycles.
fig. S19. Rate performance of Zn-C4Q batteries with a Nafion separator.
fig. S20. Galvanostatic discharge and charge curves with selected cycles at 500 mA g^{-1} and corresponding energy efficiency.
fig. S21. Cycling performance of Zn-C4Q battery using C4Q cathode with a higher conductive carbon ratio (60 wt %).
fig. S22. Exhibition of pouch cells.
fig. S23. Digital photo and SEM image of the zinc anode after cycling in pouch cells.
fig. S24. Digital photos of designed batteries after in situ UV-vis spectrum collections.
fig. S25. Selected two-dimensional UV-vis spectra.
fig. S26. ^{1}H NMR spectra of different electrolytes after cycling in batteries used for the UV-vis test.
fig. S27. Membrane potential tests.
fig. S28. EIS of Zn-C4Q batteries.
fig. S29. Electrochemical performance of aqueous Mg-C4Q batteries.
fig. S30. Structure of C4Q after uptake of three Mg ions.
table S1. Maximum specific capacity and lowest discharge/charge gap of electrodes coupled with metal zinc in aqueous batteries.

REFERENCES AND NOTES

1. B. Dunn, H. Kamath, J.-M. Tarascon, Electrical energy storage for the grid: A battery of choices. *Science* **334**, 928–935 (2011).

2. Z. Yang, J. Zhang, M. C. W. Kintner-Meyer, X. Lu, D. Choi, J. P. Lemmon, J. Liu. Electrochemical energy storage for green grid. *Chem. Rev.* **111**, 3577–3613 (2011).
3. W. I. Al Sadat, L. A. Archer, The O_2-assisted Al/CO_2 electrochemical cell: A system for CO_2 capture/conversion and electric power generation. *Sci. Adv.* **2**, e1600968 (2016).
4. T. B. Schon, B. T. McAllister, P.-F. Li, D. S. Seferos, The rise of organic electrode materials for energy storage. *Chem. Soc. Rev.* **45**, 6345–6404 (2016).
5. Q. Zhao, Z. Zhu, J. Chen, Molecular engineering with organic carbonyl electrode materials for advanced stationary and redox flow rechargeable batteries. *Adv. Mater.* **29**, 1607007 (2017).
6. K. Lin, Q. Chen, M. R. Gerhardt, L. Tong, S. B. Kim, L. Eisenach, A. W. Valle, D. Hardee, R. G. Gordon, M. J. Aziz, M. P. Marshak, Alkaline quinone flow battery. *Science* **349**, 1529–1532 (2015).
7. J. Steuber, G. Vohl, M. S. Casutt, T. Vorburger, K. Diederichs, G. Fritz, Structure of the V. *cholerae* Na^+-pumping NADH:quinone oxidoreductase. *Nature* **516**, 62–67 (2014).
8. R. H. Thomson, *Naturally Occurring Quinones IV: Recent Advances* (Chapman and Hall, 1996).
9. W. Huang, Z. Zhu, L. Wang, S. Wang, H. Li, Z. Tao, J. Shi, L. Guan, J. Chen, Quasi-solid-state rechargeable lithium-ion batteries with a calix[4]quinone cathode and gel polymer electrolyte. *Angew. Chem. Int. Ed.* **52**, 9162–9166 (2013).
10. S. Muench, A. Wild, C. Friebe, B. Häupler, T. Janoschka, U. S. Schubert, Polymer-based organic batteries. *Chem. Rev.* **116**, 9438–9484 (2016).
11. Q. Zhao, J. Wang, Y. Lu, Y. Li, G. Liang, J. Chen, Oxocarbon salts for fast rechargeable batteries. *Angew. Chem. Int. Ed.* **55**, 12528–12532 (2016).
12. J. Wang, Q. Zhao, G. Wang, F. Li, J. Chen, Enhanced adsorption of carbonyl molecules on graphene via π-Li-π interaction: A first-principle study. *Sci. China Mater.* **60**, 674–680 (2017).
13. Y. Liang, Y. Jing, S. Gheytani, K.-Y. Lee, P. Liu, A. Facchetti, Y. Yao, Universal quinone electrodes for long cycle life aqueous rechargeable batteries. *Nat. Mater.* **16**, 841–848 (2017).
14. X. Dong, L. Chen, J. Liu, S. Haller, Y. Wang, Y. Xia, Environmentally-friendly aqueous Li (or Na)-ion battery with fast electrode kinetics and super-long life. *Sci. Adv.* **2**, e1501038 (2016).
15. W. Li, J. R. Dahn, D. S. Wainwright, Rechargeable lithium batteries with aqueous electrolytes. *Science* **264**, 1115–1118 (1994).
16. H. Kim, J. Hong, K.-Y. Park, H. Kim, S.-W. Kim, K. Kang, Aqueous rechargeable Li and Na ion batteries. *Chem. Rev.* **114**, 11788–11827 (2014).
17. L. Suo, O. Borodin, T. Gao, M. Olguin, J. Ho, X. Fan, C. Luo, C. Wang K. Xu, "Water-in-salt" electrolyte enables high-voltage aqueous lithium-ion chemistries. *Science* **350**, 938–943 (2015).
18. C. Xu, B. Li, H. Du, F. Kang, Energetic zinc ion chemistry: The rechargeable zinc ion battery. *Angew. Chem. Int. Ed.* **51**, 933–935 (2012).
19. H. Pan, Y. Shao, P. Yan, Y. Cheng, K. S. Han, Z. Nie, C. Wang, J. Yang, X. Li, P. Bhattacharya, K. T. Mueller, J. Liu, Reversible aqueous zinc/manganese oxide energy storage from conversion reactions. *Nat. Energy* **1**, 16039 (2016).
20. B. Häupler, C. Rössel, A. M. Schwenke, J. Winsberg, D. Schmidt, A. Wild, U. S. Schubert Aqueous zinc-organic polymer battery with a high rate performance and long lifetime. *NPG Asia Mater.* **8**, e283 (2016).
21. J. F. Parker, C. N. Chervin, I. R. Pala, M. Machler, M. F. Burz, J. W. Long, D. R. Rolison, Rechargeable nickel–3D zinc batteries: An energy-dense, safer alternative to lithium-ion. *Science* **356**, 415–418 (2017).
22. M. H. Alfaruqi, V. Mathew, J. Gim, S. Kim, J. Song, J. P. Baboo, S. H. Choi, J. Kim, Electrochemically induced structural transformation in a γ-MnO_2 cathode of a high capacity zinc-ion battery system. *Chem. Mater.* **27**, 3609–3620 (2015).
23. D. Kundu, B. D. Adams, V. Duffort, S. H. Vajargah, L. F. Nazar, A high-capacity and long-life aqueous rechargeable zinc battery using a metal oxide intercalation cathode. *Nat. Energy* **1**, 16119 (2016).
24. N. Zhang, F. Cheng, Y. Liu, Q. Zhao, K. Lei, C. Chen, X. Liu, J. Chen, Cation-deficient spinel $ZnMn_2O_4$ cathode in $Zn(CF_3SO_3)_2$ electrolyte for rechargeable aqueous Zn-ion battery. *J. Am. Chem. Soc.* **138**, 12894–12901 (2016).
25. W. Kaveevivitchai, A. Manthiram, High-capacity zinc-ion storage in an open-tunnel oxide for aqueous and nonaqueous Zn-ion batteries. *J. Mater. Chem. A* **4**, 18737–18741 (2016).
26. B. Zhang, Y. Liu, X. Wu, Y. Yang, Z. Chang, Z. Wen, Y. Wu, An aqueous rechargeable battery based on zinc anode and $Na_{0.95}MnO_2$. *Chem. Commun.* **50**, 1209–1211 (2014).
27. G. G. Yadav, J. W. Gallaway, D. E. Turney, M. Nyce, J. Huang, X. Wei, S. Banerjee, Regenerable Cu-intercalated MnO_2 layered cathode for highly cyclable energy dense batteries. *Nat. Commun.* **8**, 14424 (2017).
28. G. G. Yadav, X. Wei, J. Huang, J. W. Gallaway, D. E. Turney, M. Nyce, J. Secor, S. Banerjee, A conversion-based highly energy dense Cu^{2+} intercalated Bi-birnessite/Zn alkaline battery. *J. Mater. Chem. A* **5**, 15845–15854 (2017).
29. Z. Liu, G. Pulletikurthi, F. Endres, A prussian blue/zinc secondary battery with a bio-ionic liquid–water mixture as electrolyte. *ACS Appl. Mater. Interfaces* **8**, 12158–12164 (2016).
30. L. Zhang, L. Chen, X. Zhou, Z. Liu, Towards high-voltage aqueous metal-ion batteries beyond 1.5 V: The zinc/zinc hexacyanoferrate system. *Adv. Energy Mater.* **5**, 1400930 (2015).
31. R. Trocoli, F. La Mantia, An aqueous zinc-ion battery based on copper hexacyanoferrate. *ChemSusChem* **8**, 481–485 (2015).
32. S.-M. Oh, S.-H. Kim, Aqueous zinc sulfate (II) rechargeable cell containing manganese (II) salt and carbon powder, U.S. Patent US6187475 B1 (2001).
33. C. Xu, Y. Chen, S. Shi, F. Kang, Rechargeable battery based on reversible manganese oxidation and reduction reaction on carbon/manganese dioxide composites, U.S. Patent US20150287988 A1 (2015).
34. F. R. McLarnon, E. J. Cairns, The secondary alkaline zinc electrode. *J. Electrochem. Soc.* **138**, 645–656 (1991).
35. D. E. Turney, J. W. Gallaway, G. G. Yadav, R. Ramirez, M. Nyce, S. Banerjee, Y.-c. K. Chen-Wiegart, J. Wang, M. J. D'Ambrose, S. Kolhekar, J. Huang, X. Wei, Rechargeable zinc alkaline anodes for long-cycle energy storage. *Chem. Mater.* **29**, 4819–4832 (2017).
36. J. McBreen, Zinc electrode shape change in secondary cells. *J. Electrochem. Soc.* **119**, 1620–1628 (1972).
37. R. E. F. Einerhand, W. Visscher, J. J. M. de Goeij, E. Barendrecht, Zinc electrode shape change. *J. Electrochem. Soc.* **138**, 7–17 (1991).
38. Y. Ito, X. Wei, D. Desai, D. Steingart, S. Banerjee, An indicator of zinc morphology transition in flowing alkaline electrolyte. *J. Power Sources* **211**, 119–128 (2012).
39. X. Wei, D. Desai, G. G. Yadav, D. E. Turney, A. Couzis, S. Banerjee, Impact of anode substrates on electrodeposited zinc over cycling in zinc-anode rechargeable alkaline batteries. *Electrochim. Acta* **212**, 603–613 (2016).
40. J. Huang, G. G. Yadav, J. W. Gallaway, X. Wei, M. Nyce, S. Banerjee, A calcium hydroxide interlayer as a selective separator for rechargeable alkaline Zn/MnO_2 batteries. *Electrochem. Commun.* **81**, 136–140 (2017).
41. L. Bai, D. Y. Qu, B. E. Conway, Y. H. Zhou, G. Chowdhury. W. A. Adams, Rechargeability of a chemically modified MnO_2/Zn battery system at practically favorable power levels. *J. Electrochem. Soc.* **140**, 884–889 (1993).
42. H. Alt, H. Binder, A. Köhling, G. Sandstede, Investigation into the use of quinone compounds-for battery cathodes. *Electrochim. Acta* **17**, 873–887 (1972).
43. B. Yang, L. Hoober-Burkhardt, F. Wang, G. K. Surya Prakash, S. R. Narayanan, An inexpensive aqueous flow battery for large-scale electrical energy storage based on water-soluble organic redox couples. *J. Electrochem. Soc.* **161**, A1371–A1380 (2014).
44. H. Liu, F. C. Strobridge, O. J. Borkiewicz, K. M. Wiaderek, K. W. Chapman, P. J. Chupas, C. P. Grey, Capturing metastable structures during high-rate cycling of $LiFePO_4$ nanoparticle electrodes. *Science* **344**, 1252817 (2014).
45. X. Wu, S. Jin, Z. Zhang, L. Jiang, L. Mu, Y.-S. Hu, H. Li, X. Chen, M. Armand, L. Chen, X. Huang, Unraveling the storage mechanism in organic carbonyl electrodes for sodium-ion batteries. *Sci. Adv.*, **1**, e1500330 (2015).
46. Z. W. Seh, J. Kibsgaard, C. F. Dickens, I. Chorkendorff, J. K. Nørskov, T. F. Jaramillo, Combining theory and experiment in electrocatalysis: Insights into materials design. *Science* **355**, eaad4998 (2017).
47. B. S. Creaven, D. F. Donlon, J. McGinley, Coordination chemistry of calix[4]arene derivatives with lower rim functionalisation and their applications. *Coord. Chem. Rev.* **253**, 893–962 (2009).
48. C. Nguyen-Trung, J. C. Bryan, D. A. Palmer, Crystal structure and thermogravimetric analysis of hexaaquazinc triflate. *Struct. Chem.* **15**, 89–94 (2004).
49. S. Er, C. Suh, M. P. Marshak, A. Aspuru-Guzik, Computational design of molecules for an all-quinone redox flow battery. *Chem. Sci.* **6**, 885–893 (2015).
50. K. J. Vetter, *Electrochemical Kinetics: Theoretical and Experimental Aspects* (Academic Press, 1967).
51. V. Augustyn, J. Come, M. A. Lowe, J. W. Kim, P.-L. Taberna, S. H. Tolbert, H. D. Abruña, P. Simon, B. Dunn, High-rate electrochemical energy storage through Li^+ intercalation pseudocapacitance. *Nat. Mater.* **12**, 518–522 (2013).
52. M. J. Frisch, G. W. Trucks, H. B. Schlegel, G. E. Scuseria, M. A. Robb, J. R. Cheeseman, G. Scalmani, V. Barone, B. Mennucci, G. A. Petersson, H. Nakatsuji, M. Caricato, X. Li, H. P. Hratchian, A. F. Izmaylov, J. Bloino, G. Zheng, J. L. Sonnenberg, M. Hada, M. Ehara, K. Toyota, R. Fukuda, J. Hasegawa, M. Ishida, T. Nakajima, Y. Honda, O. Kitao, H. Nakai, T. Vreven, J. A. Montgomery Jr., J. E. Peralta, F. Ogliaro, M. Bearpark, J. J. Heyd, E. Brothers, K. N. Kudin, V. N. Staroverov, R. Kobayashi, J. Normand, K. Raghavachari, A. Rendell, J. C. Burant, S. S. Iyengar, J. Tomasi, M. Cossi, N. Rega, J. M. Millam, M. Klene, J. E. Knox, J. B. Cross, V. Bakken, C. Adamo, J. Jaramillo, R. Gomperts, R. E. Stratmann, O. Yazyev, A. J. Austin, R. Cammi, C. Pomelli, J. W. Ochterski, R. L. Martin, K. Morokuma, V. G. Zakrzewski, G. A. Voth, P. Salvador, J. J. Dannenberg, S. Dapprich, A. D. Daniels, Ö. Farkas, J. B. Foresman, J. V. Ortiz, J. Cioslowski, D. J. Fox, *Gaussian 09 revision A.01* (Gaussian Inc., 2009).
53. J. S. Murray, K. D. Sen, *Molecular Electrostatic Potentials: Concepts and Applications* (Elsevier, 1996).

54. J. Tao, M.-L. Tong, J.-X. Shi, X.-M. Chen, S. W. Ng, Blue photoluminescent zinc coordination polymers with supertetranuclear cores. *Chem. Commun.* **0**, 2043–2044 (2000).
55. H. Stammreich, Th. T. Sans, Molecular vibrations of quinones. IV. Raman spectra of *p*-benzoquinone and its centrosymmetrically substituted isotopic derivatives and assignment of observed frequencies. *J. Chem. Phys.* **42**, 920–931 (1965).
56. Y. Morita, T. Agawa, Y. Kai, N. Kanehisa, N. Kasai, E. Nomura, H. Taniguchi, Syntheses and crystal structure of calix[4]quinone. *Chem. Lett.* **18**, 1349–1352 (1989).
57. K. A. Mauritz, R. B. Moore, State of understanding of Nafion. *Chem. Rev.* **104**, 4535–4586 (2004).
58. J. W. Choi, D. Aurbach, Promise and reality of post-lithium-ion batteries with high energy densities. *Nat. Rev. Mater.* **1**, 16013 (2016).
59. R. K. Nagarale, G. S. Gohil, V. K. Shahi, Recent developments on ion-exchange membranes and electro-membrane processes. *Adv. Colloid Interface Sci.* **119**, 97–130 (2006).
60. C. H. Hamann, A. Hamnett, W. Vielstich, *Electrochemistry* (Wiley-VCH Verlag Gmbh & Co. KGaI, 2007).

Acknowledgments
Funding: This work was supported by the National Programs for Nano-Key Project (2017YFA0206700 and 2016YFA0202500), the National Natural Science Foundation of China (21403187), and the 111 Project of Ministry of Education (B12015). **Author contributions:** Q.Z. and J.C. conceived and designed this work. W.H. and J.H. prepared C4Q. Q.Z. took the electrochemical tests. Q.Z., Y. Lu, and Z.L. carried the in situ ATR-FTIR and in situ UV-vis measurement. Q.Z., Y. Li., L. Li, and H.M. assembled the pouch cells. L. Liu carried out the DFT calculations. All authors contributed to the data analysis. Q.Z. and J.C. co-wrote the paper. J.C. directed the research. **Competing interests:** The authors declare that they have no competing interests. **Data and materials availability:** All data needed to evaluate the conclusions in the paper are present in the paper and/or the Supplementary Materials. Additional data related to this paper may be requested from the authors.

Submitted 22 June 2017
Accepted 31 January 2018
Published 2 March 2018
10.1126/sciadv.aao1761

Citation: Q. Zhao, W. Huang, Z. Luo, L. Liu, Y. Lu, Y. Li, L. Li, J. Hu, H. Ma, J. Chen, High-capacity aqueous zinc batteries using sustainable quinone electrodes. *Sci. Adv.* **4**, eaao1761 (2018).